AUT Journal of Electrical Engineering
10.22060/EEJ.2024.23380.5610

Beyond Signal Processing: A Model-Based Luenberger Observer Approach for Accurate Bearing Fault Diagnosis

Shoresh Shokoohi[1,*], Jamal Moshtagh[2]

[1]PhD Candidate, Electrical Engineering Department, University of Kurdistan, Sanandaj, Iran
[2]Professor, Electrical Engineering Department, University of Kurdistan, Sanandaj, Iran

Abstract:

Traditionally, diagnosis of bearing faults involves analyzing the frequency spectra of monitored signals, like vibration and stator current, using various signal processing techniques. However, signal-based methods for fault diagnosis often produce false alarms due to changes in load and voltage imbalances in the motor's input. Furthermore, these methods have limited performance in detecting faults at early stages and readjusting based on speed, load, and voltage levels. To overcome these challenges, this paper proposes a model-based approach for bearing fault diagnosis utilizing the Luenberger observer. The suggested model-based method compares the real behavior of the system with the estimated behavior of its nominal model, eliminating non-fault-related factors that have similar effects on both the system and its mathematical model. The efficiency of the suggested model-based bearing fault diagnosis method is validated by comparing simulation and experimental results obtained from the proposed model-based method with a recent signal-based method. The proposed method introduces a novel application of the Luenberger observer for fault detection in induction motors, offering a simple and efficient approach to diagnosing bearing faults. It uniquely distinguishes mechanical faults without direct electrical signal correlation and incorporates a systematic noise cancellation technique, enhancing robustness and accuracy under varying loads.

Keywords:

Bearing Fault Diagnosis, Luenberger Observer, Induction Motor, Current Residue

* Corresponding author, E-mail: sh.shokoohi@uok.ac.ir

10.22060/EEJ.2024.23380.5610

1. Introduction

Induction motors (IMs) are widely utilized in diverse industries due to their capacity to withstand challenging environments, wide operational spectrum, simple construction, cost efficiency, and high dependability. Despite these benefits, failures may occur in different motor parts such as bearings, rotors, and stators [1-7]. According to reports from the IEEE [8, 9], Faults related to bearings contribute to over 40% of IMs' failures. Primary issues with bearings can lead to alterations in air-gap eccentricity, shaft bending, and subsequent effects on rotor and stator functionality. Consequently, a significant demand exists for an efficient approach to detecting bearing faults.

Fig. 1 depicts the typical structure of a ball bearing, comprising an outer raceway, inner raceway, ball elements, and a cage ensuring ball spacing and preventing contact. When faults arise in bearing components like the ball, inner raceway, or outer raceway, a particular frequency identified as fault signature frequency is generated [10]. Studies show that fault signature frequencies are influenced by factors like operating speed, bearing geometry, and fault location [11]. Vibration signals are widely employed in bearing condition monitoring as they directly reflect the mechanical response resulting from defects or wear in ball bearings, caused by interactions with the inner and outer raceways [12]. Utilizing signal conditioning techniques to preprocess these signals enables the detection of probabilistic faults in bearings by comparing the spectrum analysis of the measured signal with that of a healthy bearing operating under the same speed and load conditions. However, vibration analysis has limitations, including susceptibility to background noise, sensitivity to changes in sensor mounting positions, and the associated cost of sensors. As an alternative to vibration analysis, motor current signature analysis (MCSA) has become popular [13]. MCSA involves measuring the current at the motor control centers (MCCs), eliminating the need for additional sensors or devices and the associated installation costs. In contrast to vibration analysis, in MCSA, the magnitude of the current spectral analysis at fault signature frequencies can vary at different motor loads and speeds [14]. In the MCSA analysis, because the magnitude of fault signature frequencies is often obscured among environmental noises, fault diagnosis process faces challenges. Therefore, researchers use

10.22060/EEJ.2024.23380.5610

data-driven approaches, advanced signal processing methods, and model-based techniques to reduce noise and improve the signal-to-noise ratio (SNR). Data-driven methods rely on abundant input signals for training, employing quantitative approaches like utilizing the air gap variation profile derived from an electrical model based on stator current [12].

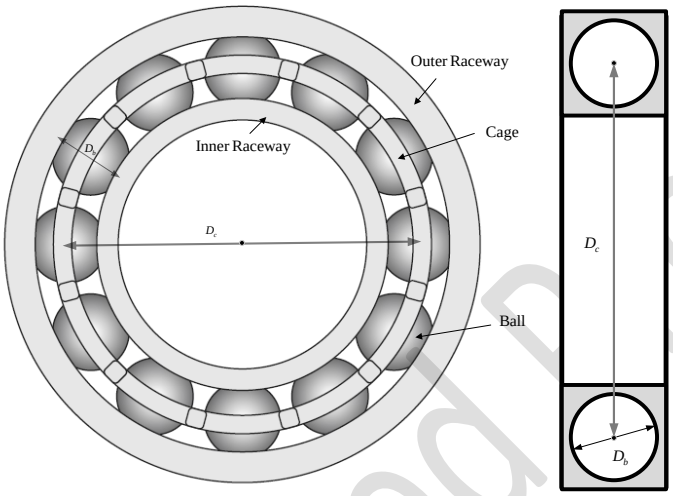

Fig. 1. Common configuration of a ball bearing

Signal-based methods encounter challenges in eliminating background noise and necessitate a thorough understanding of signal-processing techniques [1, 3, 4, 15-17]. These studies propose methods involving the time-shifting of IM's current to eliminate background noise. In [3], a technique for canceling current noise by employing time shifting is used to diminish background noise and the magnitude of multiple harmonics in the current signal. This is achieved by combining the current signal gathered with its delayed counterpart. In [4, 16], the challenge of background noise in the current signal is tackled by employing linear prediction (LP) techniques. LP method predicts and removes repetitive noise components, allowing for clearer identification of fault signatures associated with bearing faults through spectrum analysis of the filtered current signal. Leveraging the synchronized nature of the motor's three stator currents is introduced in [1, 17]. By strategically integrating these currents with time-shifting, the method cancels out background noise while retaining the fault signatures in the current spectrum. These methods enable clearer detection of bearing fault signatures in the current spectrum. Signal-based fault detection methods have limitations,

including reliance on signal analysis which may be less accurate in complex systems, limited capability for early detection, difficulty in handling intricate system dynamics, less adaptability to changes in system conditions, susceptibility to false alarms in noisy environments, and limited performance in the presence of noise or uncertain dynamics.

Model-based methods offer a potential solution, but the challenge lies in selecting an appropriate mathematical model. Model-based fault diagnosis relies on mathematical models that describe the system's behavior. These models are based on physics, engineering principles, or another domain-specific knowledge. As a result, the diagnosis can be more accurate and precise compared to signal-based or purely data-driven methods. Since Model-based methods employ dynamic system models, they can often detect faults at an early stage or even predict potential faults before they lead to system failure. This early detection capability can contribute to proactive maintenance and reduce downtime. The objective of model-based methods is to make use of all accessible information, such as input and output signals, to generate a reference signal known as the residue. The residue indicates the disparity between the outputs of a healthy process and a faulty process. When the process is fault-free, the residue is close to zero; however, it deviates from zero in the presence of a fault. The selection of an appropriate residue is vital for detecting the presence and location of a fault. A significant advantage of utilizing a model-based approach for bearing fault diagnosis is its ability to minimize false alarms during normal operation. Signal-based fault diagnosis methods are prone to false alarms caused by load changes and voltage imbalances [18]. By incorporating knowledge about the system's behavior, model-based fault diagnosis can help reduce false alarms. This is especially important in critical applications where unnecessary alarms could lead to unwarranted maintenance actions or operational disruptions. Model-based methods achieve effective noise and disturbance cancellation by comparing the measured signal with the estimated signal, thereby eliminating non-fault-related noises that affect both the model and the actual system. This automatic noise cancellation is a notable advantage of model-based methods compared to signal-based methods. Furthermore, model-based methods are not reliant on the operating point or variations in operating conditions, enhancing their

10.22060/EEJ.2024.23380.5610

robustness and applicability. The comparison of the advantages and disadvantages of all three methods has been summarized in Table 1. This table highlights that model-based fault diagnosis methods stand out for their high accuracy, precision, and ability to detect faults early, thanks to their reliance on detailed mathematical models that accurately represent system dynamics. These methods are particularly well-suited for complex systems and offer robust performance with fewer false alarms, as they can be tailored to adapt to changes in system conditions. While developing accurate models can be challenging, the advantages of model-based approaches—such as their superior reliability in complex and dynamic environments—often make them a better choice compared to signal-based and data-driven methods, which may struggle with accuracy, adaptability, and false alarms, especially in noisy or uncertain conditions.

Table 1. Comparing advantages and disadvantages of model-based, signal-based, and data-driven fault diagnosis methods

	Method / Criteria	Model-based	Signal-based	Data-driven
Advantages	*Accuracy and Precision*	High accuracy and precision due to mathematical models representing system dynamics.	Relies on signal analysis, and may be less accurate in complex systems.	Depending on data quality and quantity, and may lack precision in certain cases.
	Early Detection of Faults	Early detection and sometimes prediction of potential faults.	Limited capability for early detection, especially in dynamic systems.	Can detect anomalies and patterns but may not provide early fault detection.
	Handling Complex Systems	Well-suited for complex systems with dynamic behavior.	May struggle with intricate system dynamics.	Suitable for complex systems but depends on quality and diversity of data.
	Robustness to Changes	Can be designed to adapt to changes in system conditions.	Less adaptable to changes in system conditions.	Can adapt to changes but requires continuous learning from new data.
	Reduced False Alarms	Can help reduce false alarms by incorporating system knowledge.	This may lead to false alarms, especially in noisy environments.	Prone to false alarms, especially when trained on noisy or incomplete data.
Disadvantages		Requires accurate models, which can be challenging for some systems.	Limited performance in the presence of noise or uncertain dynamics.	Susceptible to noisy or incomplete data, and may overfit or generalize poorly.

10.22060/EEJ.2024.23380.5610

Model-based methods can be categorized into state/output observer, parameter estimation, and extended Kalman filter techniques [19-23]. They depend on a deep understanding of the physical characteristics of bearing faults and their effects on mechanical and electrical signals. While the Kalman filter and its modified versions have demonstrated advantages in fault diagnosis, they require precise specification of noise statistics [24-26]. A suggested model-based approach employs a conventional derivative-free Kalman filter for bearing fault diagnosis [19]. In [20], a comparison was made between stator current and estimated mechanical speed for model-based fault diagnosis in asynchronous drives, involving a complex extraction procedure. Other model-based methods, such as multiple coupled circuit and magnetic equivalent circuit, do not rely on observers [27-29]. In [29], a multiple coupled circuit modeling approach is introduced for simulating three-phase squirrel-cage IMs under localized bearing faults. However, it is crucial to note that this model overlooks load torque variation. A bearing model-based fault diagnosis method using airgap displacement is proposed in [12]. Its complexity and calibration challenges may arise in practical applications, particularly with varying operating conditions. A magnetic equivalent circuit is employed in [28] to investigate faulty rolling bearings. In this context, the IM model is created by segmenting uniform distribution parts into specific flux tubes. Connecting these flux tubes with nodes forms a magnetic equivalent network. Apart from its intricacy, the primary drawback of this modeling approach is its incorporation of air gap permeance between a stator and a rotor tooth, which is affected by fringing. Bearing faults impact motor performance by causing periodic radial movement of the rotor center and fluctuations in load torque. Although the influence of load torque variations on electrical signals is usually insignificant in the early stages of a bearing fault, alterations in the air gap length between the rotor and stator can modify stator current due to changes in the mutual inductance profile. However, additional research is needed to establish the precise physical model connecting vibrations to spectral components of motor current [18].

This paper introduces a pioneering approach to bearing fault diagnosis, focusing on current noise cancellation through a model-based method employing a Luenberger observer. By generating residues via a comparison of estimated and measured currents of an IM, leveraging existing stator voltage and current

information without the need for supplementary sensors, the complexity, and cost associated with bearing fault diagnosis setups are significantly mitigated. Notably, the efficiency of the proposed method is rigorously assessed across diverse load conditions, encompassing various types and severities of bearing faults: outer raceway (with two severity levels), inner raceway (with two severity levels), and ball faults. Overall, the novelty of this work resides in its capacity to offer a simplified, yet effective, model-based solution for bearing fault diagnosis that outperforms traditional methods in terms of simplicity, interpretability, and versatility. By bridging the gap between complexity and practicality, the novelty of the proposed method lies in its innovative application of the Luenberger observer for fault detection and identification in IMs. This approach introduces a simple yet efficient mathematical technique to diagnose bearing faults, distinguishing them by effectively identifying mechanical faults that do not directly correlate with electrical signals, such as stator currents. By treating bearing faults as internal disturbances, the method can accurately detect these mechanical issues. Additionally, it incorporates a systematic noise cancellation process within the Luenberger observer framework, enhancing the robustness and accuracy of fault diagnosis under varying load conditions, thereby representing a significant advancement in the field.

The following sections of the paper are structured as follows: Section 2 illustrates details of the proposed model-based approach for bearing fault diagnosis and presents the dynamic model of a single squirrel cage IM. In Section 3, a simulation test is conducted to validate the effectiveness of the proposed method as a model-based bearing fault detector. Section 4 describes the experimental benchmark employed in the study. The experimental results, demonstrate the efficacy of the proposed diagnostic approach under various faulty conditions (outer raceway, inner raceway, and ball faults), different operating points of the IM, and two levels of fault severity (low-level and high-level). Finally, in Section 5, the study's conclusions are summarized.

2. Proposed Model-Based Bearing Fault Diagnosis

10.22060/EEJ.2024.23380.5610

In this section, the overall structure of the proposed model-based method to diagnose bearing faults is presented. Also, the mathematical model of a squirrel cage IM is explained, considering the effects of bearing faults as internal disturbances that require detection.

2-1-Overall Structure of the Proposed Model-Based Bearing Fault Diagnosis Approach

Fig. 2 depicts the overall structure of the proposed model-based approach for bearing fault diagnosis. First, the input (voltage) and output (current) signals of the IM are measured using voltage and current transformer sensors, respectively, and are fed into the computer through the data acquisition system. In the subsequent stage, the measured input signals, $u(t)$, are applied to the mathematical model of the IM as inputs. The obtained output from the mathematical model, $\hat{y}(t)$, is compared with the real output signal, $y(t)$; and using the Luenberger observer method, the residue signal is generated. Finally, the fault signatures of a faulty bearing can be identified through spectrum analysis using a simple fast Fourier transform (FFT). As known in the industry, all IMs are equipped with a voltage protection system that acts to disconnect IMs from the circuit in case of voltage drop or increase to prevent damage to the IM windings. Therefore, during normal operation of the IM, the input voltage remains constant (along with inherent fluctuations of the network), and hence variations in operating points for voltage have not been considered. It is worth mentioning that all test data (including the IM's voltage) have been collected in an industrial environment in the presence of various loads such as compressors and different types of motors. Fluctuations and noise originating from the network and environment have been recorded in the voltage data, yet fault detection results have been obtained despite these factors. Regarding changes in the current operating point, for each fault, the data were stored at three different operating points (50%, 65%, and 80% of the IM's rated current), and conducted the analysis related to fault detection.

10.22060/EEJ.2024.23380.5610

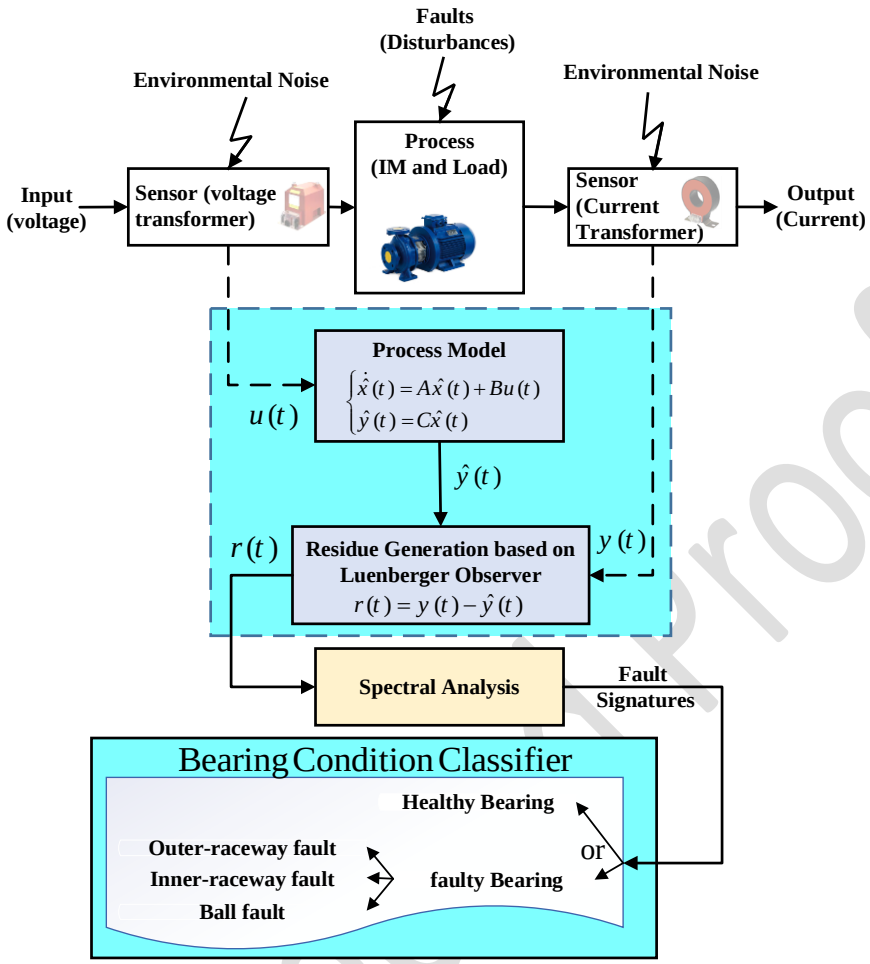

Fig. 2. Overall structure of the proposed model-based bearing fault diagnosis approach

The main innovation of the proposed method is the simplicity and ease of fault detection; So that by taking a test of a few seconds from the IM, and after transferring the IM's voltage and current data into the computer, with a simple subtraction, the proposed residue signal is obtained. Then, using a simple FFT, the bearing fault components (if any) are revealed. This is while the previous fault detection methods are usually forced to use complex signal processing techniques (signal-based) or use metaheuristics and artificial intelligence methods (data-based). The experimental results show that in addition to the visibility of the bearing fault signatures, the proposed method has been able to reduce the background noise well and automatically. In fact, by subtracting the actual output signal from the estimated output signal, the magnitude of the common frequency components between the real system and the mathematical model is

10.22060/EEJ.2024.23380.5610

reduced, as well as due to their random nature, the amplitude of the existing background noise components is reduced by the subtraction of the real output and the estimated output.

2-2-Electro-Mechanical Model of a Squirrel Cage

The *dq0* reference frame enhances fault detection in electric motors by simplifying fault signatures, decoupling fault effects, highlighting zero-sequence components, and facilitating advanced signal processing techniques. This leads to more accurate and real-time fault diagnosis, improving motor reliability and maintenance efficiency [30]. Thus, here *dq0* reference frame is used to model the IM. A fifth-order state space model is used to represent the squirrel cage IM, which includes electrical and mechanical components [30]. In the IM's equivalent circuit shown in Fig. 3, all electrical variables are referenced to the stator and shown by prime notation.

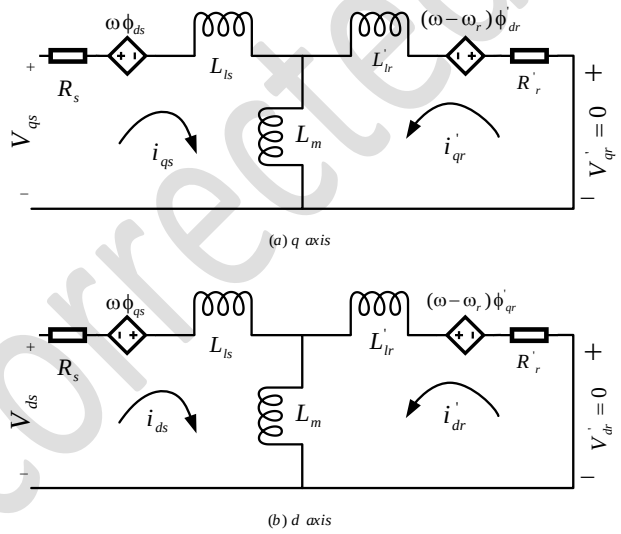

Fig. 3. Equivalent circuit of the electrical part of a squirrel cage IM

The equations representing the stator voltage in the *dq0* reference frame can be expressed as:

10.22060/EEJ.2024.23380.5610

$$\begin{cases} v_{qs} = R_s i_{qs} + \dfrac{\mathrm{d}\varphi_{qs}}{\mathrm{dt}} + \omega\varphi_{ds} \\ v_{ds} = R_s i_{ds} + \dfrac{\mathrm{d}\varphi_{ds}}{\mathrm{dt}} - \omega\varphi_{qs} \\ 0 = R'_r i'_{qr} + \dfrac{\mathrm{d}\varphi'_{qr}}{\mathrm{dt}} + (\omega - \omega_r)\varphi'_{dr} \\ 0 = R'_r i'_{dr} + \dfrac{\mathrm{d}\varphi'_{dr}}{\mathrm{dt}} - (\omega - \omega_r)\varphi'_{qr} \end{cases} \quad (1)$$

In the given equations, v represents the voltage, i represents the current, R denotes the motor resistance, ω and ω_r represent the reference frame and electrical rotor angular speeds, respectively. φ represents the flux, with subscripts d and q representing the direct and quadrature axes, and subscripts s and r denoting the stator and rotor parameters. The fluxes mentioned in Fig. 3 and Eq. (1) are defined in the following manner:

$$\begin{cases} \varphi_{qs} = L_s i_{qs} + L_m i'_{qr} \\ \varphi_{ds} = L_s i_{ds} + L_m i'_{dr} \\ \varphi'_{qr} = L'_r i'_{qr} + L_m i_{qs} \\ \varphi'_{dr} = L'_r i'_{dr} + L_m i_{ds} \end{cases} \quad (2)$$

where, L_m , L_s and L'_r are magnetizing and total stator and rotor inductances, respectively. Total stator and rotor inductances are calculated as below:

$$\begin{cases} L_s = L_{ls} + L_m \\ L'_r = L'_{lr} + L_m \end{cases} \quad (3)$$

where, L_{ls} and L'_{lr} are leakage inductances of stator and rotor, respectively. The electromagnetic torque is given by:

$$T_e = 1.5P(\varphi_{ds} i_{qs} - \varphi_{qs} i_{ds}), \quad (4)$$

where, P represents the number of pole pairs. The equations about the mechanical components (motor and load) are expressed as follows:

10.22060/EEJ.2024.23380.5610

$$\begin{cases} \dfrac{\mathrm{d}\omega_m}{\mathrm{dt}} = \dfrac{1}{J}(T_e - F\omega_m - T_m) \\ \omega_m = \dfrac{d\theta_m}{dt} \end{cases} \tag{5}$$

where, T_m represents the shaft's mechanical torque, J denotes the combined inertia coefficient of the rotor and load, and F represents the combined viscous friction coefficient of the rotor and load, ω_m is mechanical angular speed, and θ_m is rotor mechanical angle. Now, considering Eq. (1)-(5), nonlinear state space equations of a squirrel cage IM can be obtained as Eq. (6):

$$\begin{cases} \dfrac{\mathrm{d}\varphi_{qs}}{\mathrm{dt}} = -\dfrac{R_s L_r^{'}}{L_s L_r^{'} - L_m^{\,2}}\varphi_{qs} - \omega\varphi_{ds} + \dfrac{R_s L_m}{L_s L_r^{'} - L_m^{\,2}}\varphi_{qr}^{'} + v_{qs} \\ \dfrac{\mathrm{d}\varphi_{ds}}{\mathrm{dt}} = -\dfrac{R_s L_r^{'}}{L_s L_r^{'} - L_m^{\,2}}\varphi_{ds} + \omega\varphi_{qs} + \dfrac{R_s L_m}{L_s L_r^{'} - L_m^{\,2}}\varphi_{dr}^{'} + v_{ds} \\ \dfrac{\mathrm{d}\varphi_{qr}^{'}}{\mathrm{dt}} = +\dfrac{R_r^{'} L_m}{L_s L_r^{'} - L_m^{\,2}}\varphi_{qs} - (\omega - \omega_r)\varphi_{dr}^{'} - \dfrac{R_r^{'} L_s}{L_s L_r^{'} - L_m^{\,2}}\varphi_{qr}^{'} \\ \dfrac{\mathrm{d}\varphi_{dr}^{'}}{\mathrm{dt}} = +\dfrac{R_r^{'} L_m}{L_s L_r^{'} - L_m^{\,2}}\varphi_{ds} + (\omega - \omega_r)\varphi_{qr}^{'} - \dfrac{R_r^{'} L_s}{L_s L_r^{'} - L_m^{\,2}}\varphi_{dr}^{'} \\ \dfrac{\mathrm{d}\omega_m}{\mathrm{dt}} = \dfrac{3P}{2J}\left(\dfrac{L_m}{L_s L_r^{'} - L_m^{\,2}}\varphi_{qs}\varphi_{dr}^{'} - \dfrac{L_m}{L_s L_r^{'} - L_m^{\,2}}\varphi_{ds}\varphi_{qr}^{'}\right) \\ \qquad\qquad -\dfrac{F}{J}\omega_m - \dfrac{1}{J}T_m. \end{cases} \tag{6}$$

The only nonlinear term in Eq. (6) is the final term, which corresponds to the state variable of the mechanical angular speed. The mechanical angular speed can vary from its nominal value by 0% to 2% depending on the load percentage. This is due to the IM's slip, which is close to zero at no load, causing the mechanical angular speed to be close to the nominal speed. At full load, the mechanical speed is approximately 1.5% to 2% lower than the nominal speed. Since the mechanical speed changes from 100% to 98% of its nominal speed as the motor load changes from 0% to 100% of the nominal load, respectively, the change in the last state variable (mechanical speed) is less than 2% over the entire operating range of the motor. Therefore, the linearized form of the last term of Eq. (6) can be used with good approximation

10.22060/EEJ.2024.23380.5610

to represent the linearized state equations at all operating points. In continuation, the linearized state space equations around the working point X_0 are obtained as follows:

$$\begin{cases} \dot{x}_1 = -\dfrac{R_s L_r^{'}}{L_s L_r^{'} - L_m^{\,2}} x_1 - \omega x_2 + \dfrac{R_s L_m}{L_s L_r^{'} - L_m^{\,2}} x_3 + u_1 \\ \dot{x}_2 = \omega x_1 - \dfrac{R_s L_r^{'}}{L_s L_r^{'} - L_m^{\,2}} x_2 + \dfrac{R_s L_m}{L_s L_r^{'} - L_m^{\,2}} x_4 + u_2 \\ \dot{x}_3 = \dfrac{R_r^{'} L_m}{L_s L_r^{'} - L_m^{\,2}} x_1 - \dfrac{R_r^{'} L_s}{L_s L_r^{'} - L_m^{\,2}} x_3 - (\omega - \omega_r) x_4 \\ \dot{x}_4 = \dfrac{R_r^{'} L_m}{L_s L_r^{'} - L_m^{\,2}} x_2 + (\omega - \omega_r) x_3 - \dfrac{R_r^{'} L_s}{L_s L_r^{'} - L_m^{\,2}} x_4 \\ \dot{\Delta x}_5 = \dfrac{3P}{2J} \dfrac{L_m}{(L_s L_r^{'} - L_m^{\,2})} \left[\varphi_{dr0}^{'} (x_1 - \varphi_{qs0}) - \varphi_{qr0}^{'} (x_2 - \varphi_{ds0}) \right] \\ \qquad - \dfrac{3P}{2J} \dfrac{L_m}{(L_s L_r^{'} - L_m^{\,2})} \left[\varphi_{ds0} (x_3 - \varphi_{qr0}^{'}) - \varphi_{qs0} (x_4 - \varphi_{dr0}^{'}) \right] - \dfrac{F}{J} (x_5 - \omega_{m0}) - \dfrac{1}{J} u_3 \end{cases} \tag{7}$$

where,

$$X_0 = \begin{bmatrix} x_1(0) \\ x_2(0) \\ x_3(0) \\ x_4(0) \\ x_5(0) \end{bmatrix} = \begin{bmatrix} \varphi_{qs0} \\ \varphi_{ds0} \\ \varphi_{qr0}^{'} \\ \varphi_{dr0}^{'} \\ \omega_{m0} \end{bmatrix}, \text{ and } u = \begin{bmatrix} u_1 \\ u_2 \\ u_3 \end{bmatrix} = \begin{bmatrix} v_{qs} \\ v_{ds} \\ T_m \end{bmatrix}. \tag{8}$$

Note that by selecting the stator current as output as Eq. (9), the linearized state space model of a squirrel cage IM is completed.

$$\begin{cases} y_1 = i_{qs} = \dfrac{1}{L_s L_r^{'} - L_m^{\,2}} \left[L_r^{'} x_1 - L_m x_3 \right] \\ y_2 = i_{ds} = \dfrac{1}{L_s L_r^{'} - L_m^{\,2}} \left[L_r^{'} x_2 - L_m x_4 \right] \end{cases} \tag{9}$$

2-3-Designing Luenberger Observer

10.22060/EEJ.2024.23380.5610

The Luenberger observer, introduced in previous works [31-33], has been utilized for detecting various faults in induction machines, converters, and inverters. However, the primary focus of this paper is to employ the Luenberger observer for the detection of mechanical faults, specifically bearing faults, in IMs. Unlike faults that directly affect electrical signals like stator current, bearing faults do not have a direct physical relationship. Therefore, the proposed approach in this paper aims to estimate the *dq* currents using the Luenberger observer to detect the internal disturbances caused by bearing faults in IMs. The specifics of the proposed Luenberger output observer are depicted in Fig. 4.

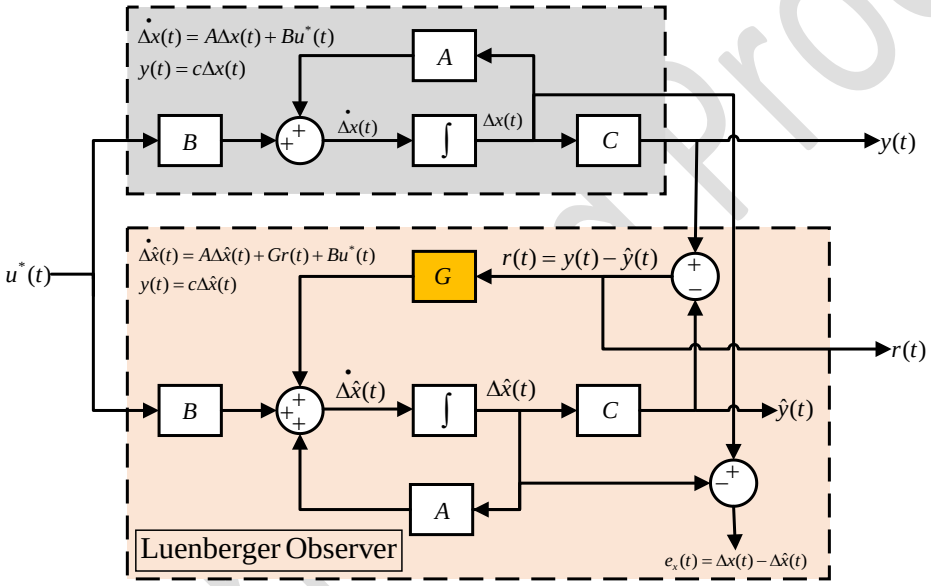

Fig. 4. The proposed Luenberger observer

The equations for the system's model and Luenberger observer, as given in [34], are as follows:

$$\text{System's model: } \begin{cases} \dot{\Delta x}(t) = A\Delta x(t) + Bu^*(t) \\ y(t) = C\Delta x(t) \end{cases} \tag{10}$$

$$\text{Luenberger observer: } \begin{cases} \dot{\Delta \hat{x}}(t) = A\Delta \hat{x}(t) + Bu^*(t) + G(y(t) - C\Delta \hat{x}(t)) \\ \hat{y}(t) = C\Delta \hat{x}(t) \end{cases} \tag{11}$$

10.22060/EEJ.2024.23380.5610

where, G is the observer's gain. A, B, and C are the state space matrixes extracted from Eq. (7) and (9). In Fig. 4, the input, $u^*(t)$, and output, $y(t)$, data are the actual voltage and current of the IM, respectively, which are already measured by the voltage and current transformer sensors. The only unknown parameter in Fig. 4 is the gain matrix, G, which is selected to achieve a satisfactory transient response. Indeed, G is designed to stabilize (push towards zero) the estimated error, which is the difference between the actual state and the estimated state, $e_x(t)$. If the state error signal $e_x(t)$ is defined as $e_x = \Delta x - \Delta\hat{x}$, then, by subtracting Eq. (10) and (11):

$$\dot{e}_x(t) = (A - GC)e_x(t). \tag{12}$$

Therefore, the observer's gain G can be calculated by placing the observer poles at desired locations, λ_i, in the complex plane using pole placement. To do this, it's sufficient that the observer poles are chosen considering factors such as system stability (having positive real parts) and convergence rate (having fast dynamics). By using the following equation:

$$\det\left(\lambda_i I - (A - GC)\right) = 0, \tag{13}$$

and the pole placement command in MATLAB (place(A',C', λ_i).')), the elements of the G matrix could be obtained. To achieve an acceptable response in terms of stability and transient response, according to the basic principles of modern control, the easiest way is to choose negative real poles with a large distance from each other. In section 3, how to choose the poles and design the gain matrix G is presented numerically.

If there is no fault (in this case, arising from a bearing fault) present (healthy bearing), $\hat{y}(t)$ closely resembles the measured system output, and any slight differences observed may stem from the presence of environmental noise in the measured output, $y(t)$, or the defined mathematical model. Therefore, in the case of a healthy bearing: $r(t)\approx 0$ and consequently: $e_x = \Delta x - \Delta\hat{x} \approx 0$. When a fault occurs within the bearing, spikes appear in the measured output, $y(t)$, during corresponding time intervals (proportional to the bearing fault frequency), leading to $r(t)\neq 0$. In such a situation, anything unrelated to the bearing fault is eliminated,

10.22060/EEJ.2024.23380.5610

and the bearing fault components persist in the residue signal, *r(t)*. Consequently, the effect of the bearing fault is reflected in the state error signal, $e_x = \Delta x - \Delta\hat{x} \neq 0$. Considering Eq. (12) and following stability principles in modern control, the condition for the proposed fault diagnosis method to be universally effective is that the matrix (*A-GC)* be Hurwitz, meaning that all its eigenvalues lie on the left side of the $j\omega$ axis (Eq. (12) remains stable). It is also preferable for these eigenvalues to exhibit a rapid transient response.

3- Simulation Results

To verify the presence of fault signatures and diminish *Gaussian* noise in frequency analysis of the output residue (current), $r_1(t) = i_d(t) - \hat{i}_d(t)$, from an IM with a faulty bearing, a simulation trial (depicted in Fig. 5) was executed using *MATLAB*'s *Simpower* toolbox. Employing a methodology akin to prior investigations [3, 10], a sequence of impulsive disturbances was induced in the load torque to consider the impact of a single-point bearing fault on the load torque profile. The simulation involved a conventional squirrel-cage IM with star configuration in stator windings. The motor was linked to a three-phase power supply with an impedance of $z=1+j0.3\Omega$ in the line. The type 6309 bearing was chosen for the simulation. The fault frequencies for this bearing type were calculated as $F_O=3.06\times F_R$, $F_I=4.95\times F_R$, and $F_B=2.00\times F_R$ [1]. Suppose the IM works at a speed of 1434 rpm (which corresponds to a frequency of 23.91 Hz). In the case of a fault in the outer raceway bearing, for example, the fault frequency (F_O) is calculated as 3.06 times the IM's working frequency, resulting in 73.18 Hz. As depicted in Fig. 5, a periodic impulsive signal, correlating with the fault signature of the outer raceway bearing, is created through the monitoring of rotor speed and its integration into the load torque. In Fig. 6, the load torque is depicted alongside a standard *Gaussian* noise with an average of 50N.m, specifically concerning the bearing afflicted with a fault in the outer raceway. The magnitudes of the impulsive components affirm a Gaussian distribution with an average of 30 and a standard deviation of 5 [1].

10.22060/EEJ.2024.23380.5610

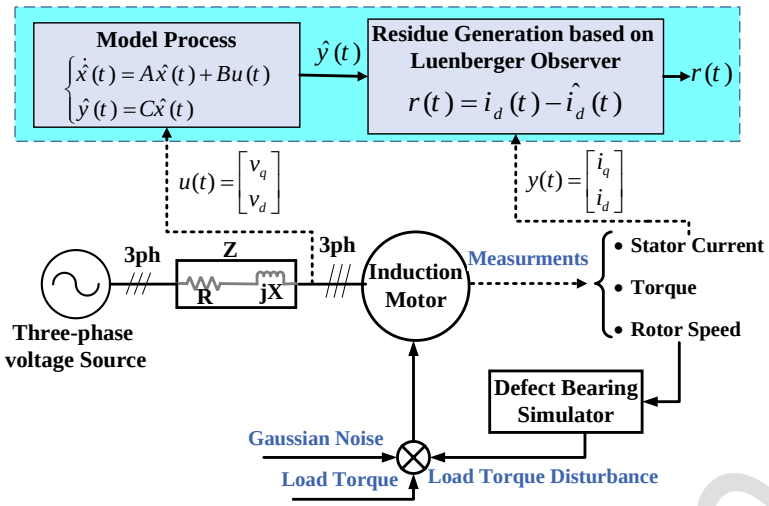

Fig. 5. Simulating the influence of bearing faults on an IM and generating residue using Luenberger

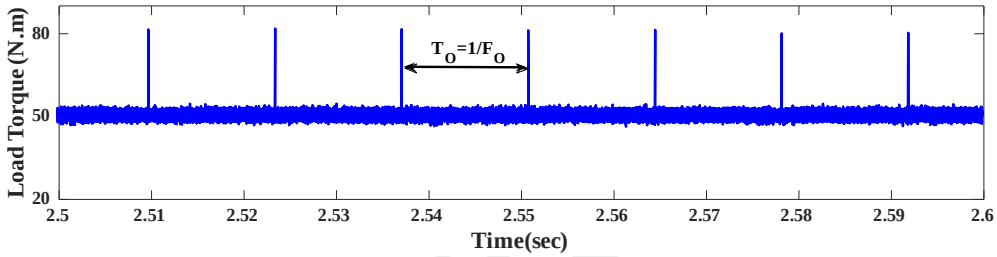

Fig. 6. Load torque profile for a faulty bearing (fault in outer raceway fault)

Considering IM parameters given in [1], Eq. (7) and (9), and following Section 2, part 2.1, an appropriate selection for desired eigenvalues (desired poles) can be as follows:

$$\lambda_i = \left[-4\times10^4 \quad -2\times10^4 \quad -1\times10^3 \quad -7\times10^2 \quad -5\times10^2\right].$$

By placing λ_i on Eq. (13), the gain matrix G is obtained as:

$$G = \begin{bmatrix} 4.53\times10^4 & 2.72\times10^8 & 3.77\times10^3 & -9.79\times10^7 & 4.53\times10^{11} \\ 3.71\times10^4 & 7.79\times10^8 & 5.37\times10^3 & -1.4\times10^8 & 1.56\times10^{11} \end{bmatrix}^T.$$

Fig. 7 illustrates the outcome of the spectrum analysis simulation for a fault in the bearing inner raceway of an IM. To assess the efficiency of the model-based approach suggested in this study in comparison to a

10.22060/EEJ.2024.23380.5610

signal-based method known as "synchronized current residue square (SCRS)" [1], the SNR index (SNRI) introduced in [1] is employed, as follows:

$$SNRI = \frac{A_{SF}}{\sqrt{\sum_{n} A_n^2}}. \tag{14}$$

A_{SF} represents the magnitude of the fault signature, while A_n signifies the magnitude of the nth sample. In Fig. 7(a) and Fig. 7(b), a comparison is made between the performance of the proposed model-based method and the SCRS method (signal-based). The results unequivocally show the successful detection of the fault frequency related to the bearing's outer raceway using the proposed model-based method. Fig. 7 illustrates the clear advantage of the proposed approach over the SCRS method. In Fig. 7(a), the results from the SCRS method are shown. The SCRS method struggles with unwanted components, including the mechanical speed frequency (f_r), double the operating frequency of the IM ($2\times f_s$), and increased background noise levels.

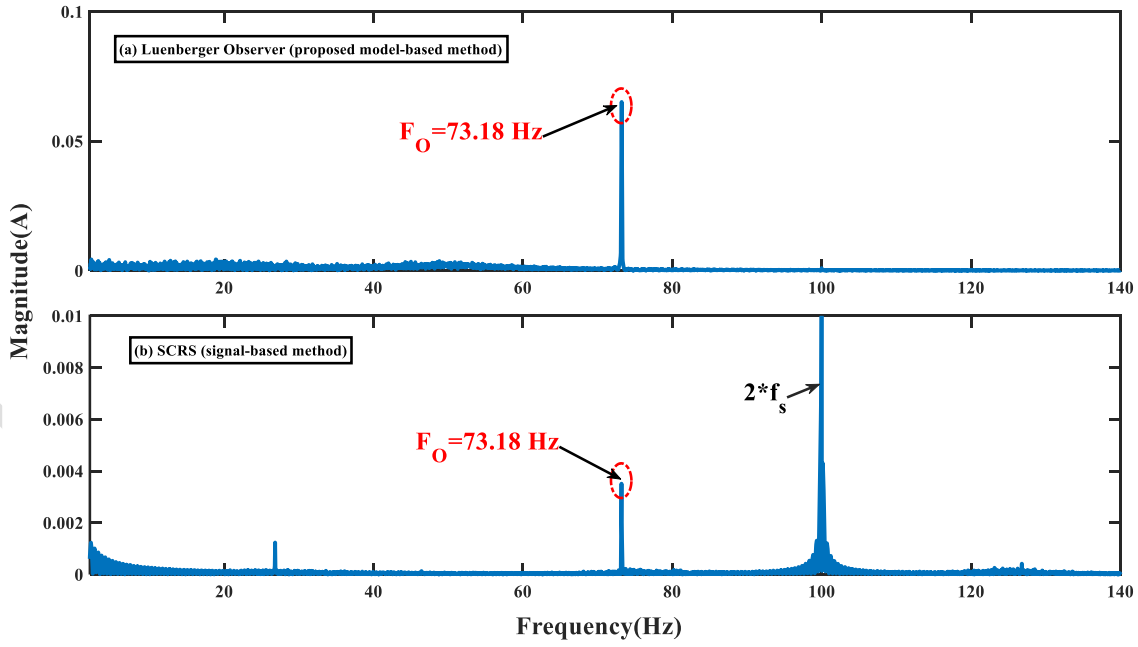

Fig. 7. Simulation results depicting spectrum analysis outcomes for a bearing fault located on the outer raceway: (a) implementation of the proposed Luenberger observer, and (b) employment of SCRS technique

This results in a less clean signal extraction. In contrast, Fig. 7(b) depicts the results from the proposed model-based method. Here, the signal is significantly cleaner with minimal unwanted components, demonstrating a more effective noise reduction. The SNRI enhancement is substantial, as shown in Table 2, which validates a significant SNRI improvement of approximately 300% with our method compared to SCRS. This improvement is primarily due to the superior handling of unwanted noise and frequency components in the proposed approach. Theses and the corresponding data underscore the robustness and effectiveness of the proposed method, providing concrete proof of its advantages over the SCRS method.

Table 2. Comparing SNR for simulating fault in outer raceway

Method	SNRI
Luenberger observer (the proposed)	0.508
SCRS [1]	0.162

4- Assessment and Verification through Experimentation

4-1- Designing Experimental Benchmark

The efficiency of the proposed model-based technique for detecting bearing faults is evaluated by analyzing a dataset collected from an experimental benchmark, as shown in Fig. 8. This benchmark consists of an IM coupled with a centrifugal pump as load with specifications given in [1]. A custom-designed data acquisition system was utilized to capture stator currents and voltages. Voltage signals were captured using the "NI 9225 300Vrms" module. Current signals, acquired via two current transformers with step-down capability, were subsequently sent to a laptop through an "NI 9227" module integrated into an "NI Compact DAQ" data acquisition chassis. The collected data was subsequently stored and processed utilizing *MATLAB* [15]. The primary focus of this investigation was on real faults occurring in SKF ball bearings with specifications given in [1], specifically the 6309 type. These faults primarily impact the outer or inner raceway, showing differences in both severity and dimensions, with diameters ranging from 1mm to 2mm. The depth of defects is 1mm in all tests. Additionally, ball defects are measuring 1mm in size. The dataset

10.22060/EEJ.2024.23380.5610

is expanded by adding three operational modes (80%, 65%, and 50% of the nominal load) over a mechanical speed span from 2908 to 2957 rpm, using a sampling rate of 51.2kHz. As depicted in Fig. 8, these changes in IM's current have been simulated by altering the percentage of opening and closing the control valve. The model-based approach is tested on the system under 18 distinct scenarios, as outlined in Table 3.

4-2- Signature of the d-axis current residue

Experimental tests are conducted to assess the performance of the proposed method, wherein the IM operates with faulty bearings at different load conditions corresponding to percentages of the nominal load (80%, 65%, and 50%). It's important to note that in all the tests, the only variation is the input operating points (voltages and currents) provided by the proposed model-based method introduced in Section 2.

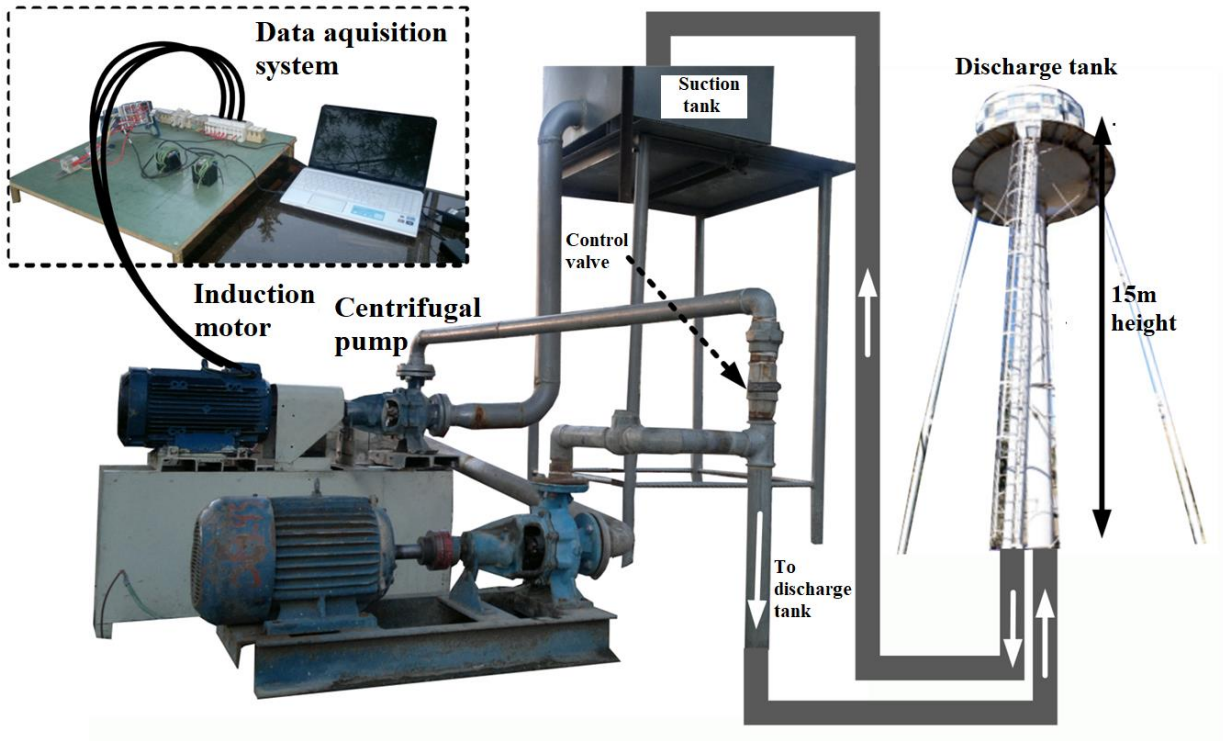

Fig. 8. The test rig and data acquisition system enclosed within the measurement panel for experimental validation [1]

Table 3. Bearing Conditions

Bearing Condition	Load percentage	label
Healthy	80	C_1
Outer raceway fault with 2mm in size	80	C_2
Outer raceway fault with 2mm in size	65	C_3
Outer raceway fault with 2mm in size	50	C_4
Outer raceway fault with 1mm in size	80	C_5
Outer raceway fault with 1mm in size	65	C_6
Outer raceway fault with 1mm in size	50	C_7
Inner raceway fault with 2mm in size	80	C_8
Inner raceway fault with 2mm in size	65	C_9
Inner raceway fault with 2mm in size	50	C_{10}
Inner raceway fault with 1mm in size	80	C_{11}
Inner raceway fault with 1mm in size	65	C_{12}
Inner raceway fault with 1mm in size	50	C_{13}
Ball fault with 1mm in size	80	C_{14}
Ball fault with 1mm in size	65	C_{15}
Ball fault with 1mm in size	50	C_{16}
Early stages of the bearing fault (due to misalignment)	100	C_{17}
Outer raceway fault with 2mm in size (measuring from MCC)	100	C_{18}

4-2-1 High-Level Fault in Outer Raceway (C_2-C_4)

In a specific scenario where the IM operates at 80% of its nominal load and a mechanical speed of 2919 rpm (C_2: F_R=48.65Hz) with a 2mm fault in the outer raceway, an anticipated spike is expected to appear at F_O=148.87Hz. Fig. 9 displays the spectrum obtained using the proposed model-based approach compared to the SCRS method for bearing fault diagnosis, specifically for the high-level outer raceway fault. The observed fault signature in the spectrum is 148.83Hz, which closely aligns with the calculated outer raceway fault signature. The primary objective of the proposed model-based method, as explained in Section 1, is to reduce noise, systematically and improve the SNR. In Fig. 9(a), a visual analysis unequivocally showcases a significant reduction in the magnitude of the noise component, compared to the SCRS method (Fig. 9(b)). This reduction contributes to improved clarity in observing the fault signature, thereby enhancing the overall visibility of the detected fault. The discernible effect on noise reduction is a testament to the efficacy of the proposed model-based method. To further validate the robustness and versatility of

10.22060/EEJ.2024.23380.5610

the proposed method, Fig. 10(a) and 10(c) present the spectra of the current residue for the IM operating at 65% and 50% of its nominal load, respectively. These different operating points simulate varying load conditions. It is noteworthy that as the load decreases, both the motor speed and the fault signature exhibit an increase. Upon scrutinizing Fig. 10, one can readily discern that the proposed model-based method consistently and successfully identifies the high-level outer raceway fault across distinct operating conditions, compared to the SCRS method (Fig. 10(b) and 10(d)). This finding emphasizes the adaptability of the method, showcasing its ability to reliably detect faults even as the motor operates at different current levels. The method's proficiency in recognizing the fault signature amidst changing operational parameters underscores its potential for widespread applicability in fault diagnosis and condition monitoring of the IM.

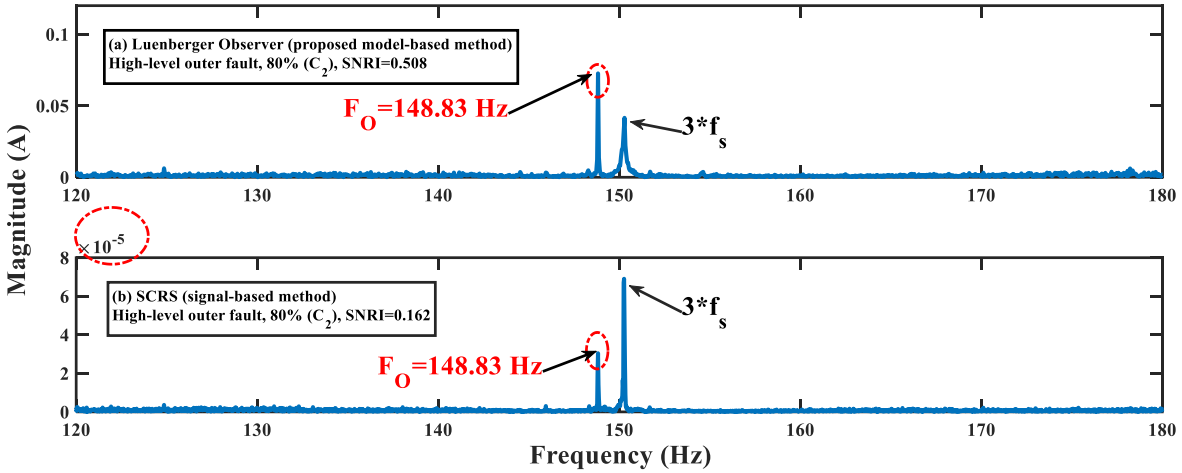

Fig. 9. Spectrum analysis of current residue: (a) Luenberger method and (b) SCRS method for the high-level fault in the outer raceway at 80% of the nominal load (test C_2)

10.22060/EEJ.2024.23380.5610

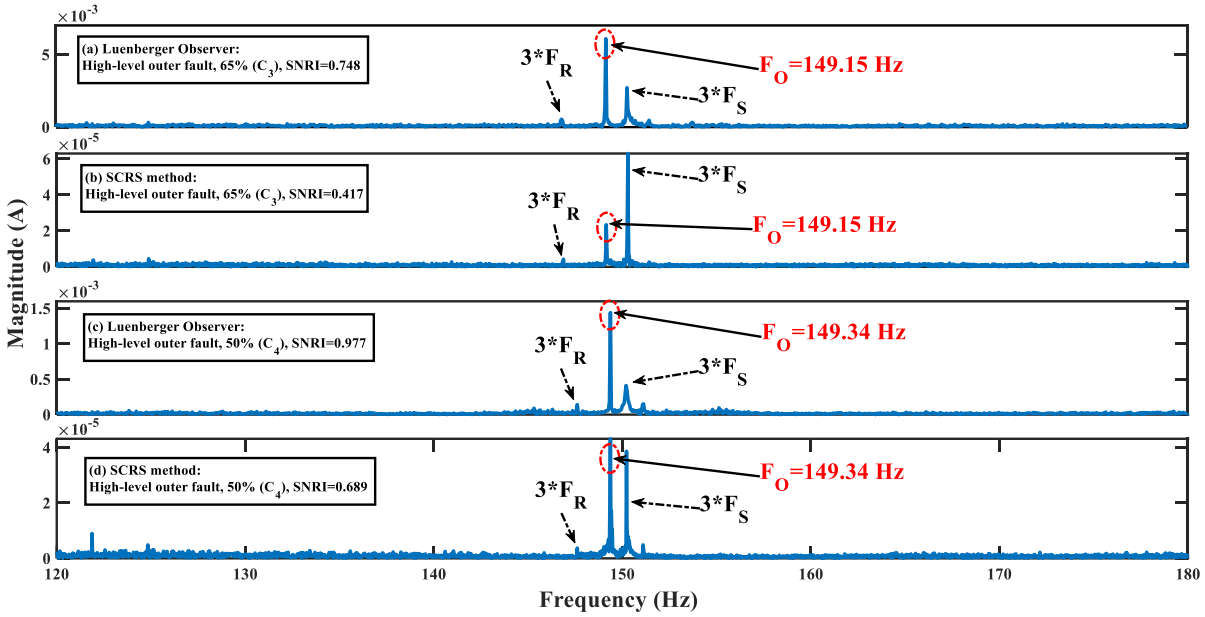

Fig. 10. Spectrum analysis of current residue: Luenberger and SCRS methods for high-level fault in the outer raceway at (a, b) 65% and (c, d) 50% of the nominal load (tests C_3 and C_4)

4-2-2 Low-Level Fault in Outer Raceway (C_5-C_7)

To assess the proficiency of the proposed approach in identifying low-level faults within the outer raceway, deliberate experimentation involves the introduction of a 1mm-sized fault deliberately placed in a different bearing, replacing the previous one. Subsequent data collection from the IM occurs while the system is operating at three distinct current levels: 80%, 65%, and 50% of its nominal load. In Fig. 11, the expected fault signatures manifest clearly across all three spectra, providing tangible evidence of the method's capability to detect and isolate faults even of a smaller magnitude. A meticulous visual examination of this figure affirms the proposed approach's efficacy, with fault signatures on the outer raceway conspicuously evident. However, in comparison to the high-level outer raceway fault examined in previous tests (C_2-C_4), it is noticeable that the magnitude of these signatures is relatively lower. This diminution in magnitude aligns with expectations, considering the inherently reduced severity of the intentionally introduced lower-level fault. The discernible contrast in the magnitude of fault signatures between high-level and lower-level faults further underscores the adaptability and sensitivity of the proposed model-based method. Despite the

10.22060/EEJ.2024.23380.5610

reduced severity of the fault, the proposed method demonstrates its ability to consistently detect and highlight fault signatures, reaffirming its utility in fault diagnosis across varying fault levels and operating conditions.

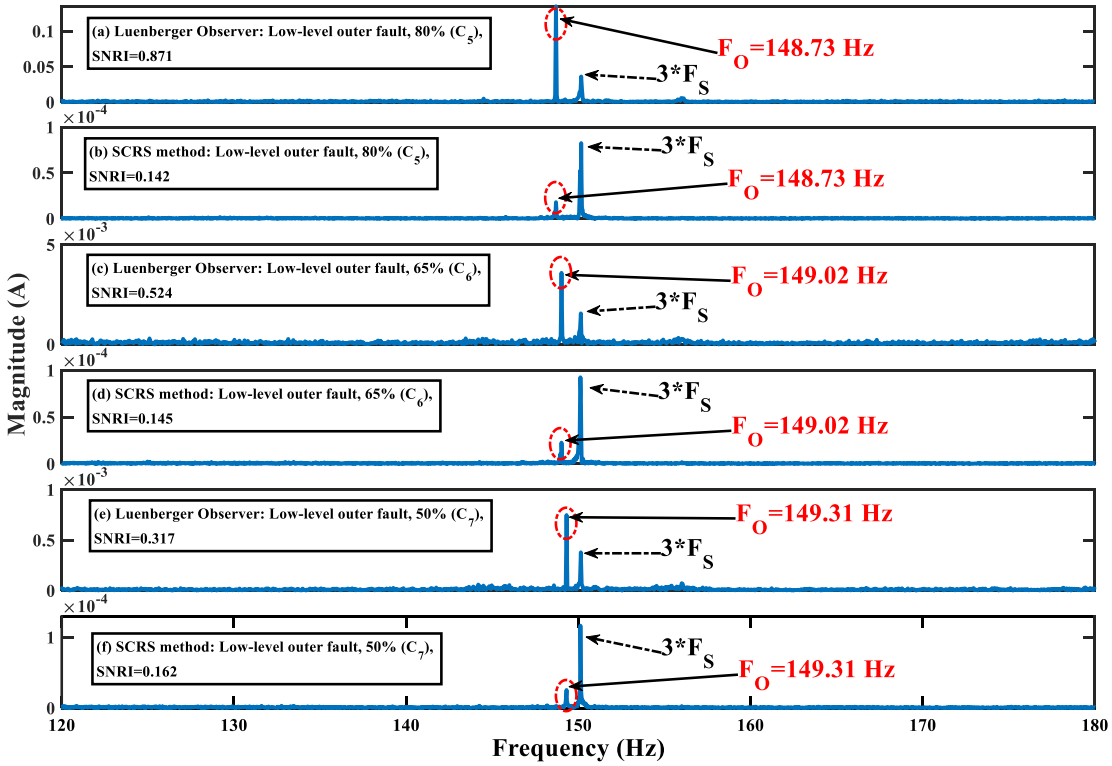

Fig. 11. Spectrum analysis of current residue: Luenberger and SCRS methods for low-level fault in the outer raceway at (a, b) 80%, (c, d) 65%, and (e, f) 50% of the nominal load (tests C_5-C_7)

4-2-3 High-Level Fault in Inner Raceway (C_8-C_{10})

In a comparable scenario where the IM operates at 80%, 65%, and 50% of its nominal load, along with mechanical speeds of 2915 rpm (C_8: F_R=48.58Hz), 2931 rpm (C_9: F_R=48.85Hz), and 2954 rpm (C_{10}: F_R=49.24Hz), featuring a 2mm fault in the inner raceway, anticipated spikes are expected to appear at F_I=240.47Hz, F_I=241.81Hz, and F_I=243.74Hz, respectively (F_I=4.95×F_R). Fig. 12 illustrates that the expected fault signatures are discernible in all three spectra, closely aligning with the calculated inner raceway fault signatures. An examination of this visual representation affirms the effectiveness of the proposed method, as the fault signatures on the inner raceway are prominently visible. Fig. 12 unmistakably

10.22060/EEJ.2024.23380.5610

demonstrates that in all three tests (C_8-C_{10}), the SNR index in the proposed method surpasses that of the SCRS method, and the fault signature frequency is more prominently and observable.

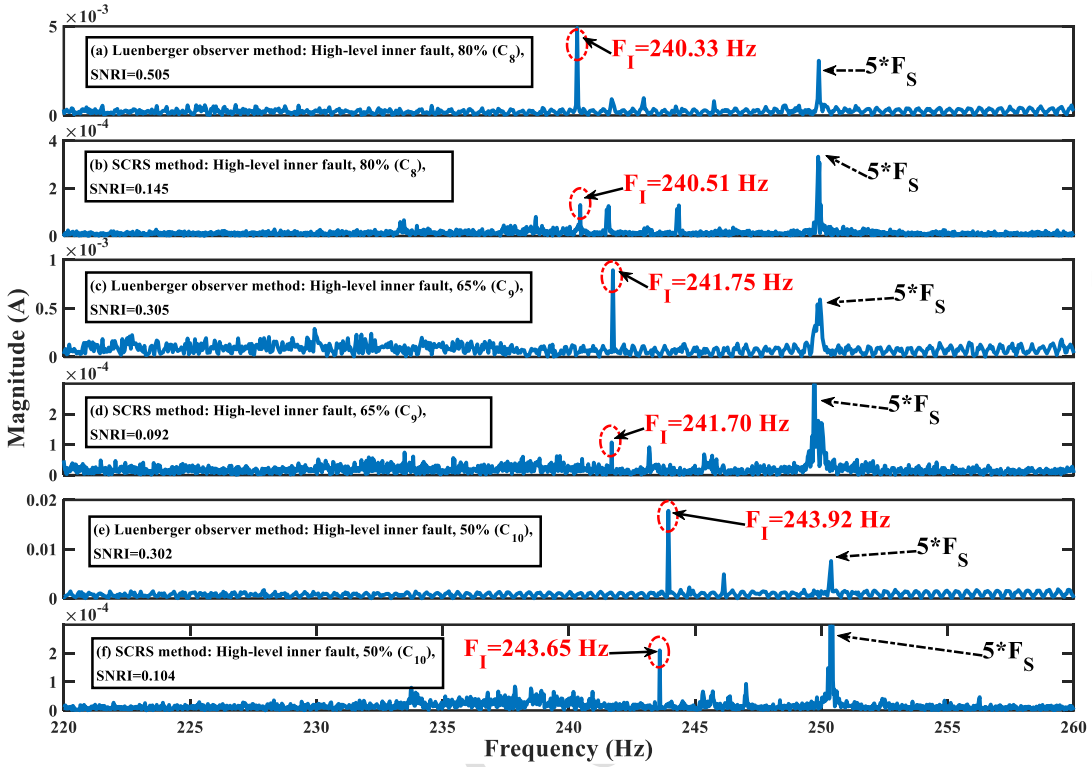

Fig. 12. Spectrum analysis of current residue: Luenberger and SCRS methods for high-level fault in the inner raceway at (a, b) 80%, (c, d) 65%, and (e, f) 50% of the nominal load (tests C_8-C_{10})

4-2-4 Low-Level Fault in Inner Raceway (C_{11}-C_{13})

In the subsequent experiment, a meticulously placed deliberate single-point fault, measuring 1mm in size, is introduced with precision into the inner raceway of the bearing. This deliberate introduction of a fault in a specific location allows for a targeted assessment of the proposed model-based method's capability to identify and characterize inner raceway faults. Consider the example when the IM operates at 80% of its nominal load (test C_{11}). In this scenario, the IM's shaft rotational frequency, denoted as F_R, is calculated to be 48.49Hz, equivalent to a mechanical speed of 2909 rpm. Consequently, an anticipated spike at F_I=4.95×F_R=240.02Hz is expected to manifest in the spectrum. Fig. 13(a) presents the spectrum obtained from the proposed model-based method under this specific condition. Remarkably, the observed fault

10.22060/EEJ.2024.23380.5610

signature closely aligns with the calculated inner raceway fault signature, registering at 239.97Hz. This precise correspondence between the observed and calculated frequencies serves as compelling evidence of the method's accuracy in pinpointing the location and nature of the inner raceway fault. Expanding on these findings, Fig. 13(c) and 13(e) are included to furnish additional evidence substantiating the efficacy of the proposed model-based method across a spectrum of operational conditions. These figures showcase the method's consistent and reliable performance in detecting and characterizing faults even as the IM operates under diverse current levels. The wealth of evidence presented in these spectra reinforces the method's adaptability and robustness in fault detection, particularly in the nuanced identification of inner raceway faults within the bearing. This underscores the method's potential applicability in real-world scenarios where precise fault diagnosis is crucial for operational integrity and maintenance decision-making.

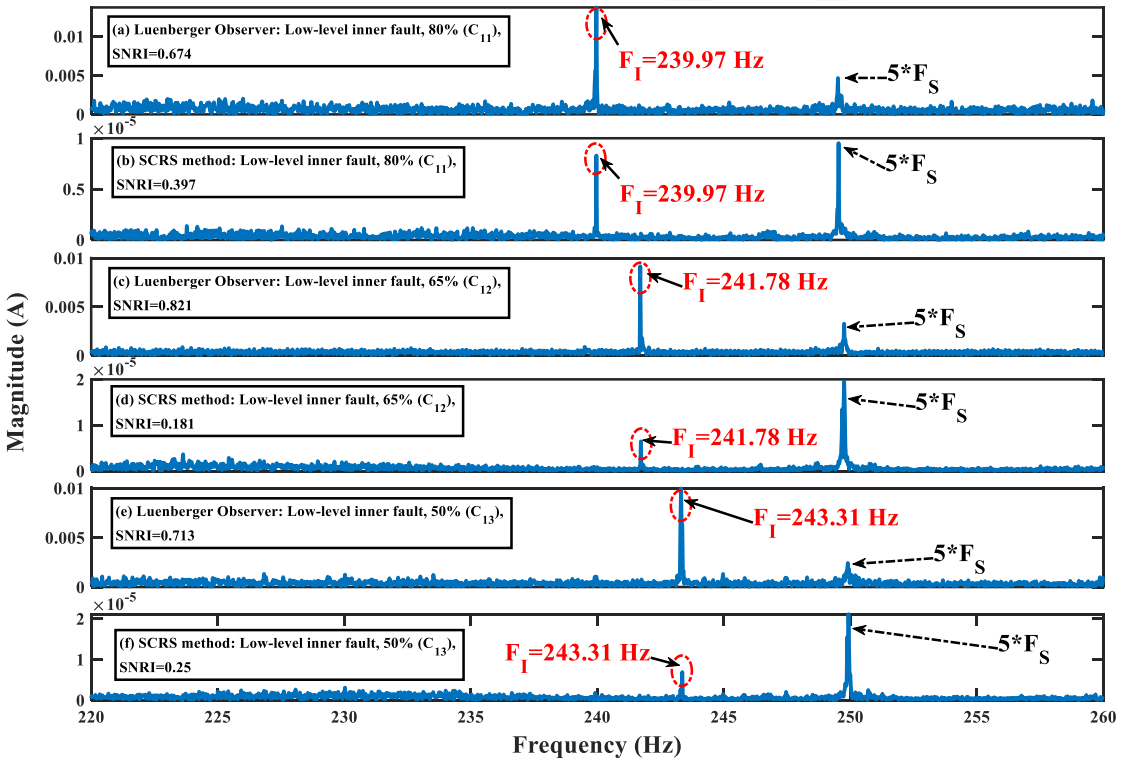

Fig. 13. Spectrum analysis of current residue: Luenberger and SCRS methods for low-level fault in the inner raceway at (a, b) 80%, (c, d) 65%, and (e, f) 50% of the nominal load (tests C_{11}-C_{13})

4-2-5 Ball Fault (C_{14}-C_{16})

10.22060/EEJ.2024.23380.5610

In another experimental scenario, a precise single-point fault, deliberately introduced at 1mm in size, is strategically placed in the ball of the bearing. This deliberate manipulation allows for a focused evaluation of the proposed model-based method's capability to accurately identify and characterize faults located in the ball component of the bearing. Consider the instance when the IM operates at 80% of its nominal load (C_{14}). In this case, the F_R is calculated to be 48.61Hz, corresponding to a mechanical speed of 2916 rpm. Consequently, an expected spike at F_B=2.00×F_R=97.22Hz is anticipated in the spectrum. Fig. 14(a) presents the spectrum acquired from the proposed model-based method under this specific operating condition. Impressively, the observed fault signature closely aligns with the calculated ball fault signature, registering at 97.19Hz. This precise correspondence serves as compelling evidence of the method's accuracy in identifying and characterizing faults specifically located in the ball component of the bearing. To fortify the reliability of these results, Fig. 14(c) and 14(e) are included, offering additional validation of the proposed model-based method's effectiveness at the remaining two operating points. These figures underscore the method's consistent and robust performance in fault detection, reinforcing its versatility across a range of operational conditions. The observed fault signatures across various scenarios further attest to the method's capability to reliably identify faults in different components of the bearing, supporting its potential application in diverse industrial settings where nuanced fault detection is critical for ensuring machinery reliability and performance.

10.22060/EEJ.2024.23380.5610

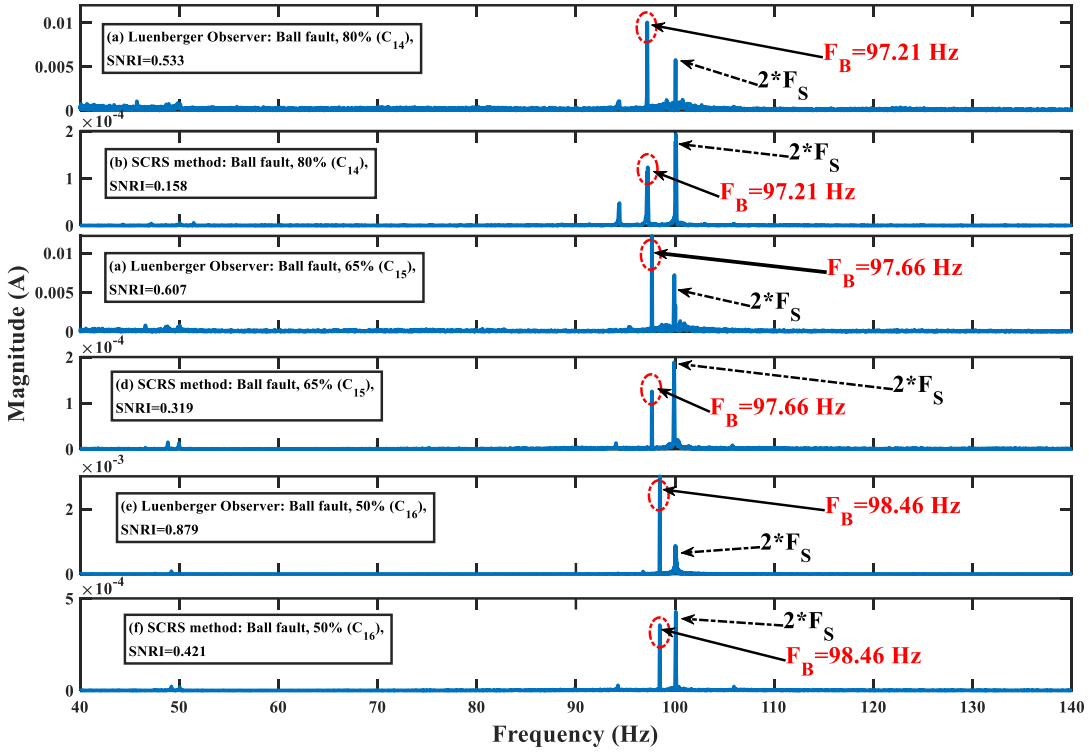

Fig. 14. Spectrum analysis of current residue: Luenberger and SCRS methods for ball fault at (a, b) 80%, (c, d) 65%, and (e, f) 50% of the nominal load (tests C_{14}-C_{16})

4-2-6 Further Assessment of Proposed Method Performance

To test the effectiveness of the proposed method for weak faults, a different test (condition C_{17}) was conducted. Typically, one of the reasons for the onset of bearing fault is the misalignment between the IM and the pump. Therefore, the data for this test pertains to a bearing that has operated for 500 hours under conditions where there is a 2mm parallel misalignment between the motor and the pump, running at full load. By analyzing the IM data under the mentioned misalignment condition, the effectiveness of the proposed method in the early detection of bearing faults can be better understood. Fig. 15 shows the spectrum of this test with the application of the proposed method: (a) for a healthy bearing (test C_1), and (b) for the bearing in condition C_{17}. As depicted in Fig.15(a), the fault signatures of the bearing (outer, inner, and ball faults) are not observed, indicating the correct identification of the bearing's healthy condition. In Fig. 15(b), the fault signatures of the ball and the outer raceway of the bearing can be seen,

10.22060/EEJ.2024.23380.5610

albeit with a low magnitude, indicating the weak intensity of the fault due to the misalignment between the motor and the pump, which is causing degradation of the ball's outer surface and consequently, the bearing's outer raceway surface. This test demonstrates the effectiveness of the proposed method in detecting faults at their early stages.

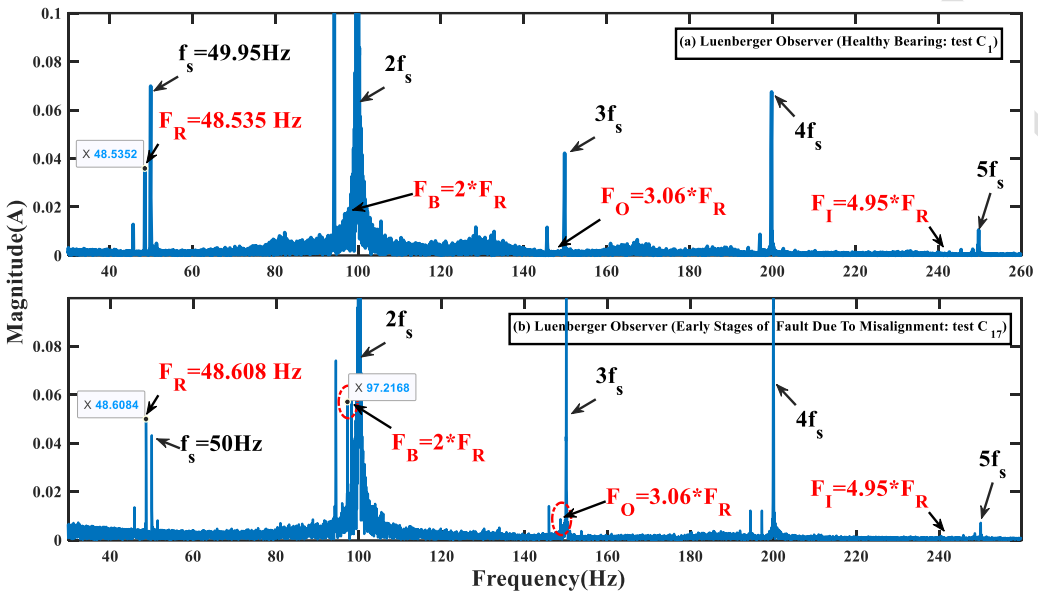

Fig. 15. Spectrum analysis of current residue: Luenberger method (a)healthy bearing (test C_1), and (b) early stages of fault due to misalignment (test C_{17})

4-2-7 Robust Assessment

Considering the diversity of faults (outer raceway, inner raceway, and ball faults), various working conditions (50%, 65%, and 80% of the nominal load of IM), and the proposed model-based method applied to two types of fault severity (1mm and 2mm-sized faults) at the tests C_2-C_{16}, the robustness of the suggested model-based method has been extensively examined. To assess how well the suggested model-based method performs in real-world scenarios, a distinct test (test C_{18}) was carried out. The data were gathered within the MCC of a pump station, located more than 100 meters away from the original benchmark site, to gauge its robustness. Within the MCC, there was a mix of loads, such as lighting and electro-pumps, adding complexity to the field. The data collected within the MCC exhibited a reduced SNR due to the

10.22060/EEJ.2024.23380.5610

relatively minor fault signatures and the potential for noise disruption via the electrical cord. During this experiment, the IM worked at full capacity and maximum operating stresses, presenting a single fault occurring at the outer raceway of the bearing with dimensions of 2 mm in diameter and depth. Fig. 16 presents the outcomes of the proposed method in comparison with the SCRS method.

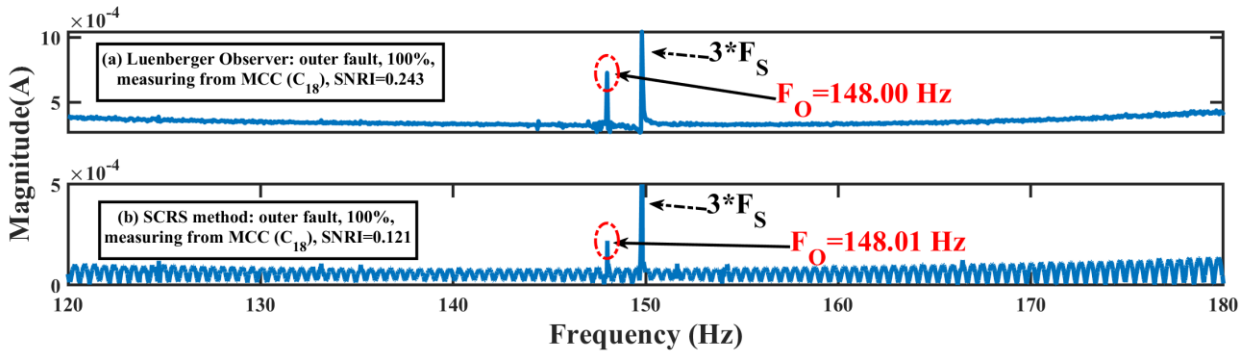

Fig. 16. Spectrum analysis of current residue: Luenberger and SCRS methods for outer raceway fault, at 50% of the nominal load, measuring from MCC (test C_{18})

4-3- Comparison with previous works

To better demonstrate the effectiveness of the proposed method, Table 4 presents a comparative overview of the SNRI index between the proposed model-based method, spectral kurtosis (SK) [2], Teager-Kaiser energy operator (TKEO) [5], linear prediction (LP) [4], time shifting (TS) [3], Fractional Linear Prediction (FLP) [16], and SCRS [1] methods on the tests C_2-$C_{18,}$ highlighting the effectiveness of the proposed model-based method. In Table 4, the asterisk (*) indicates that the specified method cannot identify the type of fault.

4-4-Performance metrics

To quantitatively verify the performance of the proposed model-based method using quantitative analysis, an additional 42 tests were conducted (in addition to the 18 tests intended in Table 3), resulting in a total of 60 tests categorized as follows: 20 tests with healthy bearings, 20 tests with outer raceway faults, 10 tests with inner raceway faults, and 10 tests with ball faults. These tests evaluated the performance of two fault

10.22060/EEJ.2024.23380.5610

detection methods: Luenberger observer (the proposed method)) and SCRS [1] in identifying four bearing states: healthy (class 0), outer fault (class 1), inner fault (class 2), and ball fault (class 3).

Table 4. Comparison of the SNR in the current noise cancellation methods for all three fault types

		Method / *%Load*	*SK [2]*	*TKEO [5]*	*LP [4]*	*TS [3]*	*FLP [16]*	*SCRS [1]*	*Luenberger Observer (proposed)*
SNRI Value	*High-Level Outer Raceway Fault*	C_2=80%	0.007	0.036	0.004	0.059	0.132	0.162	***0.508***
		C_3=65%	0.006	0.022	0.003	0.043	0.212	0.417	***0.748***
		C_4=50%	0.015	0.015	0.003	0.068	0.571	0.689	***0.977***
	Low-Level Outer Raceway Fault	C_5=80%	0.001	0.056	0.002	0.079	0.173	0.142	***0.871***
		C_6=65%	0.006	0.045	0.005	0.082	0.111	0.145	***0.524***
		C_7=50%	0.008	0.034	0.004	0.078	0.091	0.162	***0.317***
	High-Level Inner Raceway Fault	C_8=80%	*	0.010	0.005	0.110	0.121	0.145	***0.505***
		C_9=65%	*	0.009	0.003	0.076	0.095	0.092	***0.305***
		C_{10}=50%	*	0.006	0.002	0.063	0.087	0.104	***0.302***
	Low-Level Inner Raceway Fault	C_{11}=80%	*	0.155	0.080	0.196	0.243	0.397	***0.674***
		C_{12}=65%	*	0.052	0.055	0.063	0.126	0.181	***0.821***
		C_{13}=50%	*	0.082	0.051	0.093	0.342	0.25	***0.713***
	Ball Fault	C_{14}=80%	0.030	*	0.011	0.017	0.123	0.158	***0.533***
		C_{15}=65%	0.035	*	0.023	0.027	0.075	0.319	***0.607***
		C_{16}=50%	0.079	*	0.013	0.016	0.298	0.421	***0.879***
	Weak ball fault (due to misalignment)	C_{17}=100%	*	*	*	*	*	*	***0.095***
	High-Level Outer Raceway Fault (measuring from MCC)	C_{18}=100%	*	*	*	*	*	0.121	***0.243***

A confusion matrix [35] is used to summarize the comparison results (see Fig. 17). Fig. 17(a) shows that out of the 40 tests conducted on faulty bearings, the proposed method correctly identified 39 as faulty and misclassified 1 as healthy. Meanwhile, the SCRS method identifies 35 tests as faulty and incorrectly predicts 5 tests as healthy (Fig. 17(b)). The matrix demonstrates that the proposed method effectively differentiates between healthy and faulty bearings. Correct predictions are positioned along the diagonal of the matrix, making it straightforward to visually identify any prediction errors, which appear as values outside the diagonal. The comparative charts of evaluation metrics: precision, recall, specificity, and accuracy [35] for both methods are shown in Fig. 18. The results indicate that the proposed model-based method generally outperforms the SCRS method across all evaluated metrics. For class 0 (healthy state), the proposed method shows a higher precision (0.95 vs. 0.78), specificity (0.97 vs. 0.88), and accuracy

10.22060/EEJ.2024.23380.5610

(0.95 vs. 0.88), while both methods have the same recall (0.90). In class 1 (outer fault), the proposed method achieves perfect recall (1.00) and higher overall metrics than SCRS, which had a recall of 0.90. Both methods perform similarly with identical metrics for class 2 (inner fault). However, for class 3 (ball fault), the proposed method exhibits perfect precision, recall, specificity, and accuracy, while SCRS shows a lower recall (0.80). These findings, illustrated in Fig. 17 and Fig. 18, suggest that the proposed model-based method provides more reliable and consistent performance in bearing fault detection compared to the SCRS, particularly in achieving higher precision, which is critical for minimizing false positives and achieving a balanced performance.

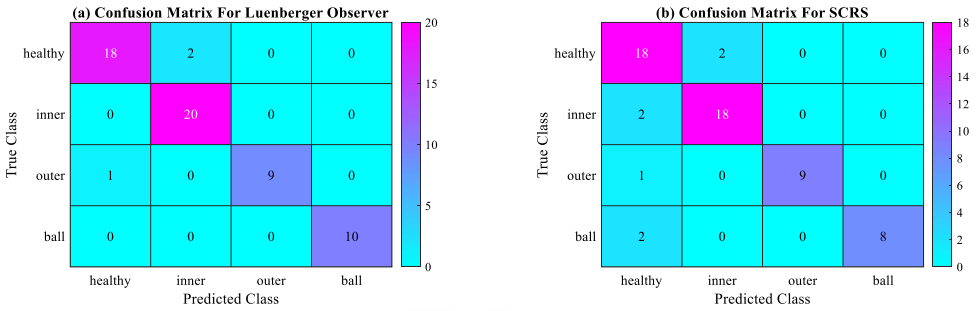

Fig. 17. Comparative analysis of confusion matrices for Luenberger observer (proposed) and SCRS methods

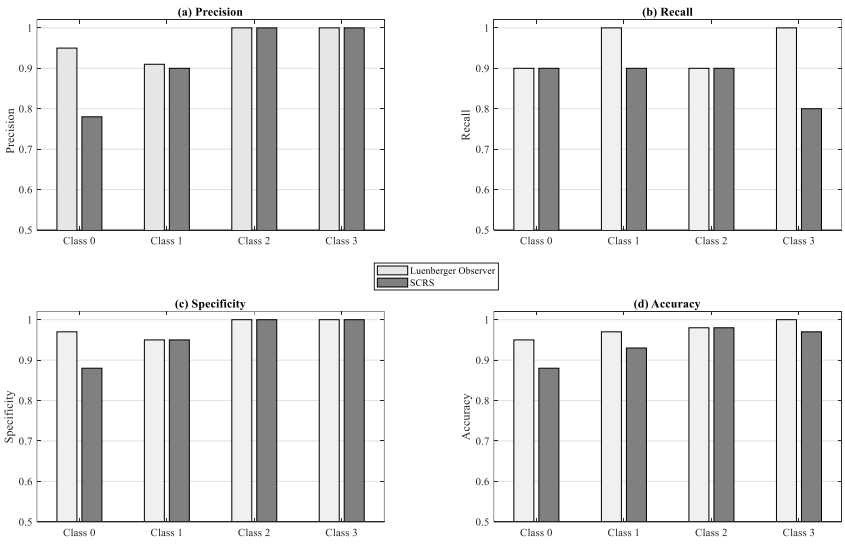

Fig. 18. Comparative charts of evaluation metrics: (a) precision, (b) recall, (c) specificity, and (d) accuracy for Luenberger observer (proposed) and SCRS methods

10.22060/EEJ.2024.23380.5610

5- Conclusion

This paper introduces a robust model-based approach for the detection of bearing faults in IMs operating under diverse loads and challenging industrial conditions. The diagnostic strategy utilizes a Luenberger observer to generate current residues, allowing the extraction of fault signatures associated with the outer raceway, inner raceway, and ball faults. To validate the efficacy of our proposed method, comprehensive tests were conducted across three distinct operating points, intentionally introducing three types of bearing faults (outer raceway, inner raceway, and ball). Moreover, tests for outer raceway and inner raceway faults were conducted at both high and low severity levels. The results demonstrate the success of the proposed model-based approach in effectively addressing the complexities of bearing fault diagnosis across different operating conditions and varying degrees of fault severity.

The proposed method, using the Luenberger observer, efficiently diagnoses bearing faults in IMs by distinguishing mechanical faults without relying on electrical signals. The integration of noise cancellation enhances robustness and accuracy, making this approach a significant advancement in fault detection. Unlike conventional methods that often rely on complex signal processing techniques; also, compared to traditional model-based methods, which often require intricate mathematical models and precise parameter estimation, the proposed approach offers a simpler and more practical solution. By utilizing a Luenberger observer, the method circumvents the need for complex models and extensive parameter tuning, thus reducing computational overhead and enhancing applicability across diverse operating conditions. In contrast to data-driven techniques, such as deep learning, which rely heavily on vast amounts of training data and intricate feature selection, the proposed method offers a more transparent and interpretable approach. Rather than depending solely on data patterns, the method leverages fundamental principles of motor operation and bearing fault characteristics, resulting in a more intuitive and physically meaningful diagnostic process.

6- Nomenclature

IM	Induction motor
MCSA	Motor current signature analysis
MCC	Motor control center
SNR	Signal-to-noise ratio
LP	Linear prediction
FFT	Fast Fourier transform
SCRS	Synchronized current residue square
SNRI	Signal-to-noise ratio index
SK	spectral kurtosis
TKEO	Teager-Kaiser energy operator
TS	time shifting
FLP	Fractional Linear Prediction
F_R	Rotor mechanical frequency
F_O	Outer raceway fault frequency
F_I	Inner raceway fault frequency
F_B	Ball fault frequency
D_b	Ball diameter
D_c	Pitch diameter
f_s	Supply frequency

References

[1] S. Nazari, S. Shokoohi, J. Moshtagh, A Current Noise Cancellation Method Based on Integration of Stator Synchronized Currents for Bearing Fault Diagnosis, IEEE Transactions on Instrumentation and Measurement, (2023) 1-1.
[2] V.C. Leite, J.G.B. da Silva, G.F.C. Veloso, L.E.B. da Silva, G. Lambert-Torres, E.L. Bonaldi, L.E.d.L. de Oliveira, Detection of localized bearing faults in induction machines by spectral kurtosis and envelope analysis of stator current, IEEE Transactions on Industrial Electronics, 62(3) (2014) 1855-1865.
[3] F. Dalvand, S. Dalvand, F. Sharafi, M. Pecht, Current noise cancellation for bearing fault diagnosis using time shifting, IEEE Transactions on Industrial Electronics, 64(10) (2017) 8138-8147.
[4] F. Dalvand, M. Kang, S. Dalvand, M. Pecht, Detection of Generalized-Roughness and Single-Point Bearing Faults Using Linear Prediction-Based Current Noise Cancellation, IEEE Transactions on Industrial Electronics, 65(12) (2018) 9728-9738.

[5] M. Pineda-Sanchez, R. Puche-Panadero, M. Riera-Guasp, J. Perez-Cruz, J. Roger-Folch, J. Pons-Llinares, V. Climente-Alarcon, J.A. Antonino-Daviu, Application of the Teager–Kaiser energy operator to the fault diagnosis of induction motors, IEEE Transactions on energy conversion, 28(4) (2013) 1036-1044.
[6] L.A.E. Noussaiba, F. Abdelaziz, ANN-based Fault Diagnosis of Induction Motor under Stator Inter-Turn Short-Circuits and Unbalanced Supply Voltage, ISA transactions, (2023).
[7] J.M. Ramírez-Sanz, J.-A. Maestro-Prieto, Á. Arnaiz-González, A. Bustillo, Semi-supervised learning for industrial fault detection and diagnosis: A systemic review, ISA transactions, (2023).
[8] P.F. Albrecht, J.C. Appiarius, R.M. McCoy, E.L. Owen, D.K. Sharma, Assessment of the Reliability of Motors in Utility Applications - Updated, IEEE Transactions on Energy Conversion, EC-1(1) (1986) 39-46.
[9] Report of Large Motor Reliability Survey of Industrial and Commercial Installations, Part I, IEEE Transactions on Industry Applications, IA-21(4) (1985) 853-864.
[10] F. Dalvand, A. Kalantar, M.S. Safizadeh, A Novel Bearing Condition Monitoring Method in Induction Motors Based on Instantaneous Frequency of Motor Voltage, IEEE Transactions on Industrial Electronics, 63(1) (2016) 364-376.
[11] R.A. Collacott, Vibration Monitoring and Diagnosis: Techniques for cost-effective plant maintenance, G. Godwin, 1979.
[12] S. Zhang, B. Wang, M. Kanemaru, C. Lin, D. Liu, M. Miyoshi, K.H. Teo, T.G. Habetler, Model-based analysis and quantification of bearing faults in induction machines, IEEE Transactions on Industry Applications, 56(3) (2020) 2158-2170.
[13] R.R. Schoen, T.G. Habetler, F. Kamran, R. Bartfield, Motor bearing damage detection using stator current monitoring, IEEE transactions on industry applications, 31(6) (1995) 1274-1279.
[14] B. Yazici, G.B. Kliman, W.J. Premerlani, R.A. Koegl, G.B. Robinson, A. Abdel-Malek, An adaptive, on-line, statistical method for bearing fault detection using stator current, in: IAS'97. Conference Record of the 1997 IEEE Industry Applications Conference Thirty-Second IAS Annual Meeting, IEEE, 1997, pp. 213-220.
[15] F. Dalvand, A. Kalantar, S. Shokoohi, H. Bevrani, Time-domain bearing condition monitoring in induction motors using instantaneous frequency of motor voltage, in: 2014 Smart Grid Conference (SGC), 2014, pp. 1-7.
[16] K. Xu, X. Song, A Current Noise Cancellation Method Based on Fractional Linear Prediction for Bearing Fault Detection, Sensors, 24(1) (2023) 52.
[17] A. Kalantar, M.S. Safizadeh, F. Dalvand, Time Synchronization and Integration of Bearing Fault Impacts upon Stator Currents, Electric Power Components and Systems, 51(19) (2023) 2284-2292.
[18] P.P. Harihara, K. Kyusung, A.G. Parlos, Signal-based versus model-based fault diagnosis-a trade-off in complexity and performance, in: 4th IEEE International Symposium on Diagnostics for Electric Machines, Power Electronics and Drives, 2003. SDEMPED 2003., 2003, pp. 277-282.
[19] S.S.S.R.S. Duvvuri, Model-Based Bearing Fault Detection in Induction Motors Under Speed Varying Conditions, in: 2018 8th IEEE India International Conference on Power Electronics (IICPE), 2018, pp. 1-6.
[20] B. Trajin, J. Regnier, J. Faucher, Comparison between stator current and estimated mechanical speed for the detection of bearing wear in asynchronous drives, IEEE Transactions on Industrial Electronics, 56(11) (2009) 4700-4709.
[21] L. Yi, T. Sun, W. Yu, X. Xu, G. Zhang, G. Jiang, Induction motor fault detection by a new sliding mode observer based on backstepping, Journal of Ambient Intelligence and Humanized Computing, 14(9) (2023) 12061-12074.
[22] G. Postal, J. Gyselinck, F. Belie, M. Kinnaert, Model-based interturn short-circuit fault detection and isolation in 3-phase PMSMs with flux-linkage estimation, in: 12th International Conference on Power Electronics, Machines and Drives (PEMD 2023), IET, 2023, pp. 315-322.
[23] M. Romdhane, M. Naoui, A. Mansouri, PMSM Inter-Turn Short Circuit Fault Detection Using the Fuzzy-Extended Kalman Filter in Electric Vehicles, Electronics, 12(18) (2023) 3758.

[24] M. Zhong, T. Xue, S.X. Ding, A survey on model-based fault diagnosis for linear discrete time-varying systems, Neurocomputing, 306 (2018) 51-60.
[25] A. Rahimi, K.D. Kumar, H. Alighanbari, Fault estimation of satellite reaction wheels using covariance based adaptive unscented Kalman filter, Acta Astronautica, 134 (2017) 159-169.
[26] H. Jiang, G. Liu, J. Li, T. Zhang, C. Wang, K. Ren, Model based fault diagnosis for drillstring washout using iterated unscented Kalman filter, Journal of Petroleum Science and Engineering, 180 (2019) 246-256.
[27] Y. Gao, X. Liu, J. Xiang, FEM Simulation-Based Generative Adversarial Networks to Detect Bearing Faults, IEEE Transactions on Industrial Informatics, 16(7) (2020) 4961-4971.
[28] Q. Han, Z. Ding, X. Xu, T. Wang, F. Chu, Stator current model for detecting rolling bearing faults in induction motors using magnetic equivalent circuits, Mechanical Systems and Signal Processing, 131 (2019) 554-575.
[29] M. Ojaghi, M. Sabouri, J. Faiz, Analytic model for induction motors under localized bearing faults, IEEE Transactions on energy conversion, 33(2) (2017) 617-626.
[30] P.C. Krause, O. Wasynczuk, S.D. Sudhoff, S. Pekarek, Analysis of electric machinery and drive systems, Wiley Online Library, 2002.
[31] I. Jlassi, J.O. Estima, S.K. El Khil, N.M. Bellaaj, A.J.M. Cardoso, Multiple open-circuit faults diagnosis in back-to-back converters of PMSG drives for wind turbine systems, IEEE Transactions on Power Electronics, 30(5) (2014) 2689-2702.
[32] I. Jlassi, J.O. Estima, S.K. El Khil, N.M. Bellaaj, A.J.M. Cardoso, A robust observer-based method for IGBTs and current sensors fault diagnosis in voltage-source inverters of PMSM drives, IEEE Transactions on Industry Applications, 53(3) (2016) 2894-2905.
[33] A. Mahmoudi, I. Jlassi, A.J.M. Cardoso, K. Yahia, M. Sahraoui, Inter-Turn Short-Circuit Faults Diagnosis in Synchronous Reluctance Machines, Using the Luenberger State Observer and Current's Second-Order Harmonic, IEEE Transactions on Industrial Electronics, 69(8) (2021) 8420-8429.
[34] D. Luenberger, An introduction to observers, IEEE Transactions on Automatic Control, 16(6) (1971) 596-602.
[35] C.M. Bishop, N.M. Nasrabadi, Pattern recognition and machine learning, Springer, 2006.